Catena 170 (2018) 129–140

Contents lists available at ScienceDirect

Catena

journal homepage: www.elsevier.com/locate/catena

Combining 3D data and traditional soil erosion assessment techniques to study the effect of a vegetation cover gradient on hillslope runoff and soil erosion in a semi-arid catchment

Sayjro K. Nouwakpo[a,*], Mark A. Weltz[b], Colleen H.M. Green[c], Awadis Arslan[a]

[a] University of Nevada Reno, Department of Natural Resources and Environmental Science, Reno, NV, USA
[b] U.S. Department of Agriculture, Agriculture Research Service, Great Basin Rangelands Research Unit, Reno, NV, USA
[c] U.S. Department of the Interior, Bureau of Land Management, National Operation Center, Denver, CO, USA

ARTICLE INFO

Keywords:
Rangeland
Erosion
Hydrology
Sediment transport
Microtopography
Digital elevation model
Dem
Structure from motion
Sfm

ABSTRACT

In this paper, we examine the effect of vegetation on soil erosion, runoff generation and sediment transport on saline rangeland hillslopes. Rainfall simulations were conducted at a fixed 114 mm/h intensity on 6 m × 2 m erosion plots with varying degrees of vegetation. Plots were grouped into three categories (L, M and H) based on their canopy cover (L: < 5%, M: 5–19%, H: > 19%) and selected to limit variations in slope across canopy cover groups. Runoff and sediment samples were combined with three dimensional (3D) reconstruction data used to monitor soil surface microtopographic changes. Runoff initiation was significantly delayed on the L plots but cumulative runoff after 20 min of rainfall simulation indicated a positive effect of vegetation on infiltration processes. Cumulative sediment after 20 min of rainfall was similar across vegetation cover categories. The 3D data suggest that vegetation reduced net sediment delivery from the plots by primarily increasing opportunities for deposition while marginally affecting gross soil erosion. Plots with H vegetation cover experienced lower 3D-estimated erosion volumes but average erosion depth on L plots was lower than that on plots with M and H vegetation covers. Lower runoff volumes on M and H plots may have been compensated by greater runoff erosivity on these plots as runoff was concentrated in a narrower inter-patch space compared to L plots. This study highlights the need for an increased integration between traditional runoff measurement techniques and 3D reconstruction methods.

1. Introduction

Soil erosion and runoff on rangelands have historically been perceived as processes that adversely impact the proper functioning of rangeland ecosystems through loss of soil and water resources (e.g., Chartier and Rostagno, 2006; Herrick et al., 2006; Turnbull et al., 2012; Whitford et al., 1995). Nevertheless, soil erosion and runoff generation are often accompanied with water and sediment redistribution along the rangeland hillslope with potentially positive outcomes on rangeland function. Schlesinger et al. (1990) even proposed that sparsely vegetated rangelands may rely on resource (water, sediments and nutrients) redistribution during episodic events (rainfall, runoff, wind events) to ensure higher production than achievable by average annual inputs. According to these authors, an indication of such dependence of sparsely vegetated rangeland on resource redistribution is the observation that shrubs were more productive along intermittent streambeds and in local areas of water accumulation. Other studies supporting coupling between resource redistribution and rangeland ecosystem sustainability include modeling efforts from Buis and Veldkamp (2008), field observations, and rainfall simulation experiments showing strong decays in runoff with hillslope length by others (e.g., Bergkamp, 1998; Cerda, 1997; Puigdefabregas et al., 1999).

Abbreviations: CDR, Ratio of 3D-estimated volume of deposition over erosion in channels; CumQ, Cumulative runoff volume (L); CumQ20, Cumulative runoff volume (L) recorded the first 20 min of rainfall; CumS, Cumulative soil loss (kg); CumS20, Cumulative soil loss (kg) recorded the first 20 min of rainfall; CVD, Total volume of deposition estimated with 3D reconstruction in channels; CVE, Total volume of erosion estimated with 3D reconstruction in channels; CZD, Average depth of deposition estimated with 3D reconstruction in channels; CZE, Average depth of erosion estimated with 3D reconstruction in channels; Q_{ss}, Steady state runoff discharge (mm/h); Rdur, Rainfall duration; Ro. Dur, Runoff duration; Sed, Sediment concentration (g/L); SDR, Sediment delivery ratio; TDR, Ratio of 3D-estimated volume of deposition over erosion; TTR, Time elapsed between the start of rainfall and the initiation of runoff; TVD, Total volume of deposition estimated with 3D reconstruction; TVE, Total volume of erosion estimated with 3D reconstruction; TZD, Average depth of deposition estimated with 3D reconstruction; TZE, Average depth of erosion estimated with 3D reconstruction

* Corresponding author at: University of Nevada Reno, Department of Natural Resources and Environmental Science, Reno, NV, USA.
E-mail address: snouwakpo@unr.edu (S.K. Nouwakpo).

https://doi.org/10.1016/j.catena.2018.06.009
Received 23 October 2016; Received in revised form 6 June 2018; Accepted 7 June 2018

Most laboratory and field research on the effect of vegetation on runoff and soil erosion processes suggest an inverse albeit non-linear relationship between plant cover and runoff and sediment production (e.g., Cerdan et al., 2002; Nicolau et al., 1996; Polyakov et al., 2016; Rogers and Schumm, 1991) and this perception forms the foundation of rangeland erosion modeling (Nearing et al., 2011). At the patch scale, vegetation has a direct shielding effect against raindrop impact, reducing rainfall energy available for soil detachment (e.g., Abrahams et al., 1995; Parsons et al., 1992; Rostagno and Delvalle, 1988; Wainwright et al., 2000) and this shielding effect is further reinforced by the presence of litter and other vegetation debris under plant canopies (e.g., Gholami et al., 2013; Wang et al., 2014). Rainfall simulation experiments by Rogers and Schumm (1991) showed a quasi-linear inverse relationship between vegetative cover and sediment yield until a threshold of 15% vegetative cover is reached where vegetation and sediment yield appeared decoupled. Nicolau et al. (1996) noted that in addition to vegetative cover, another major controlling factor of runoff is the spatial arrangement of vegetation clumps as shrub circumventions by flow paths resulted in decreased runoff. In addition, when runoff concentrates in channels, the presence of litter and other vegetative materials contribute to the total soil shear strength (Blackburn, 1975; Cammeraat and Imeson, 1998; Pierson et al., 2014; Pierson et al., 2010; Williams et al., 2014a), reducing concentrated flow erosion. Increased soil loss associated with decrease in flow path tortuosity was also found on degraded tussock grasslands (Tongway and Ludwig, 1997). Other effects include the increase in effective soil surface roughness that reduces runoff velocity and promotes deposition (e.g., Al-Hamdan et al., 2013; Emmett, 1970; Pierson et al., 2007; Pierson et al., 2009; Siepel et al., 2002; Wainwright et al., 2000), reduction in total runoff through interception storage (Carlyle-Moses, 2004; Owens et al., 2006) and enhanced infiltration (Bhark and Small, 2003; Caldwell et al., 2012; Nulsen et al., 1986). In general, these factors and other processes opposing the delivery of resources (water, sediment and nutrients) across scales are lumped into the concept of connectivity (e.g., Bracken and Croke, 2007; Williams et al., 2014a; Williams et al., 2016a).

It is clear that vegetation interacts with sediment and water transport processes in a source-sink interrelationship that varies as a function of vegetation community type (Magliano et al., 2015; Merino-Martín et al., 2012). Studies in hydrodynamic research on the effect of vegetation patches on fluvial processes (e.g., Meire et al., 2014; Rominger and Nepf, 2011) showed that flow deflections by vegetation patches are associated with deposition features upstream patches. Furthermore, these regions of deposition can promote new vegetation growth in the long-term (Meire et al., 2014). On rangelands, it is important to understand how vegetation patches influence water and sediment transport processes to devise land management techniques that target specific processes to achieve desired outcomes. Traditional techniques used to evaluate the effect of vegetation on transport processes often involve quantifying changes in runoff or sediment concentration with hillslope length (Bergkamp, 1998; Cerda, 1997; Puigdefabregas et al., 1999). However, the complexity arising from scale and spatial connectivity of rangeland erosion and hydrologic processes (e.g., Pierson et al., 2009; Sadeghi et al., 2013; Williams et al., 2016b) render the interpretation of such vegetation-induced changes in runoff and sediment concentration difficult especially in the presence of active rills. Techniques that can explicitly and simultaneously quantify erosion, deposition in relation to hydrologic input and vegetation cover are likely to yield better results in linking vegetation to sediment transport processes.

The emergence and accessibility of three dimensional (3D) reconstruction techniques now offer new opportunities to study sediment transport processes in a more spatially explicit manner (Gillan et al., 2016; Nouwakpo et al., 2016a; Prosdocimi et al., 2017). When these 3D techniques are combined with traditional soil erosion and runoff measurement methods, interactions between vegetation and sediment transport processes can be examined with greater details (Nouwakpo et al., 2017). Nouwakpo et al. (2017), found that vegetation controlled surface processes by constraining runoff into the bare interspace between vegetation plants and promoting deposition. Nevertheless, Nouwakpo et al.'s (2017) study was not specifically designed to study vegetation effect on surface processes as other factors such as slope, vegetation type, litter and soil type varied between sites and treatments. The aim of the current study is to clarify the role of vegetation cover amount in controlling detachment, transport and redistribution of sediment on sparsely vegetated rangelands by combining soil surface 3D change information with traditional erosion assessment methodologies during simulated rainfall events. Unlike the Nouwakpo et al. (2017) paper, experiments in the current study were conducted on a single site using one rainfall intensity with only vegetation cover varied between treatments.

2. Materials and methods

2.1. Study site and plot selection

The study site is located near the city of Ferron in the state of Utah, USA (Fig. 1). Soils at the site are developed in the Mancos Shale geologic formation with high soil salinity and erodibility. The soil is mapped as a complex of Chipeta series (clayey, mixed, active, calcareous, mesic, shallow typic torriorthents) and Badland. This soil was derived from weathered clayey shale, forming a paralithic restrictive layer at a depth varying between 0.1 and 0.5 m. Soil texture at the site was classified as silt loam (USDA Taxonomy) with 11.5% sand, 66.7% silt and 21.8% clay. The study site is part of the warm central desertic basins and plateaus of the United States. Average annual precipitation in this region ranges between 150 and 255 mm mostly occurring as convective thunderstorms during the period of July to September. Vegetation at the study site was dominated by the shrub *Atriplex corrugata*.

Three hillslopes were identified at the study site to represent low (L, canopy cover < 5%), medium (M, 5% < canopy cover < 19%) and high (H, canopy cover > 19%) vegetation covers. Potential hillslopes were selected by visually identifying three contrasting densities of *Atriplex corrugata* on the site (Fig. 2). Hillslopes of similar slopes and soil characteristic were picked to minimize confounding effects of these factors on soil erosion processes. Four plots were randomly selected on each hillslope, giving a total of twelve plots to conduct the rainfall simulation experiments.

2.2. Materials

The experimental protocol used in this study is similar to that used in previous studies at the same site (e.g., Cadaret et al., 2016; Nouwakpo et al., 2017) except that in the current study, only one rainfall intensity was applied to each plot. On each plot selected, a rainfall of 114 mm/h intensity was applied. This intensity was determined from precipitation frequencies published by the United States National Oceanic and Atmospheric Administration (Atlas 14) (Bonnin et al., 2006) by selecting the 25-year storm and multiplying its 5-minute depth by 12 to get a depth per hour. Rainfall was simulated with the computer-controlled Walnut Gulch Rainfall Simulator (Paige et al., 2004). The simulator nozzles were pressured at 55 kPa at a height of 2.44 m which allow raindrops to approach terminal raindrop velocity (Paige et al., 2004).

Ground and vegetation cover on each plot were assessed using a laser point frame (VanAmburg et al., 2005). The laser point measurement consisted in a laser line vertically projected on the ground and visually tracked by an observer to determine intersecting vegetation canopy and ground cover (litter, bare soil, rocks, and biological crusts). In our study this laser measurement was made on a 0.5 m × 0.1 m grid (or 220 sample points) per plot and provided information on canopy cover, litter cover, rock content and the fraction of bare ground.

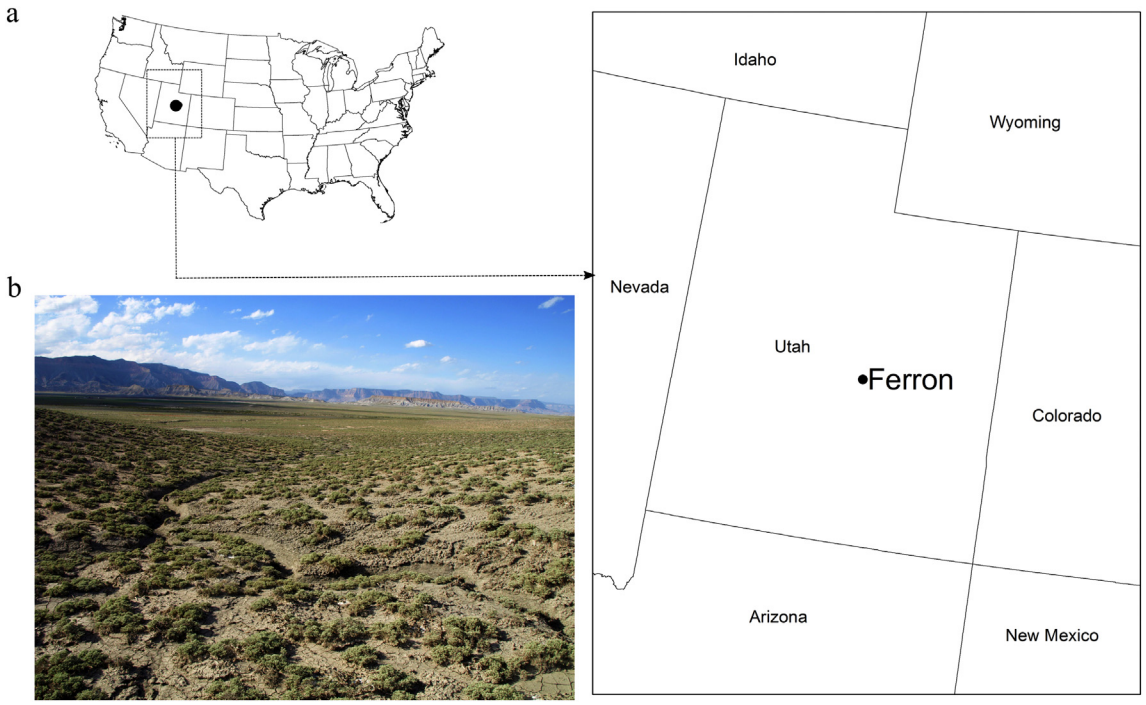

Fig. 1. Map showing the city of Ferron, Utah in the United States (a) and a ground photograph of the study site (b).

A Canon EOS Rebel T3i (Canon Inc., Tokyo, Japan) single lens reflex camera was used to take pre- and post-rainfall simulation pictures for 3D reconstruction. The camera was fitted with a 20 mm lens with the autofocus setting disabled. Pictures were taken with the camera held by an operator who walked along the perimeter of each plot to take a series of overlapping oblique pictures of the plot in a convergent configuration (Fig. 3). An average of 344 pictures were needed to cover the plot area.

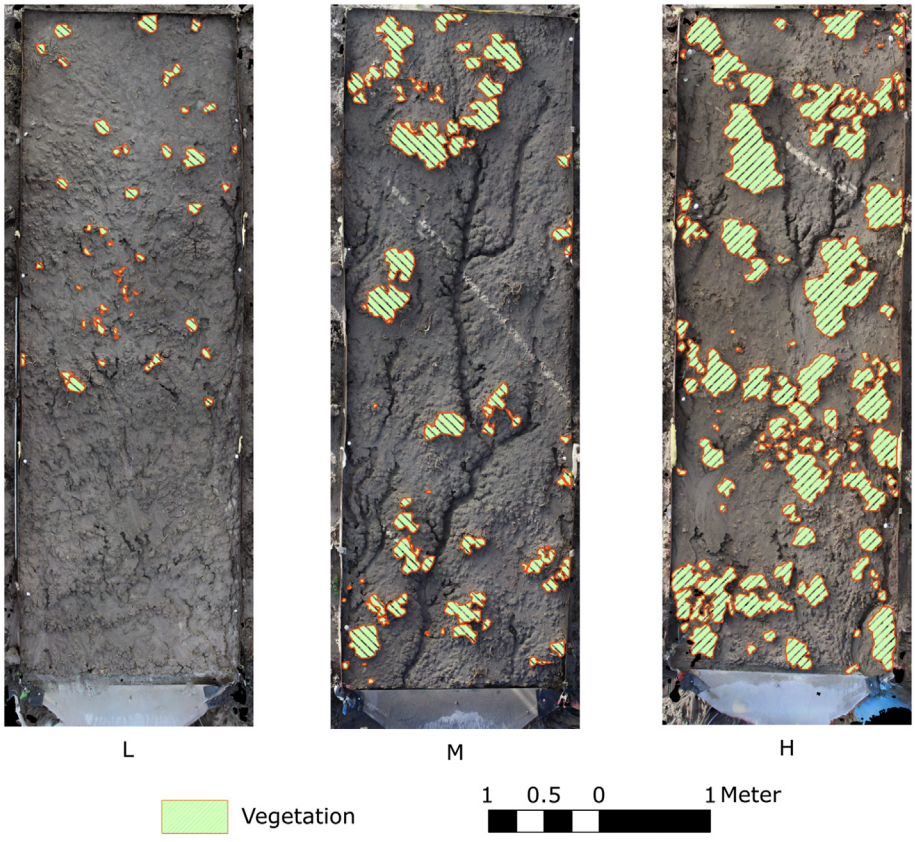

Fig. 2. Example of synoptic view of post-erosion plots with low (L), medium (M) and high (H) vegetation canopy covers. Plots were classified as L if canopy cover < 5%, M if 5% < canopy cover < 19% and H if canopy cover > 19%.

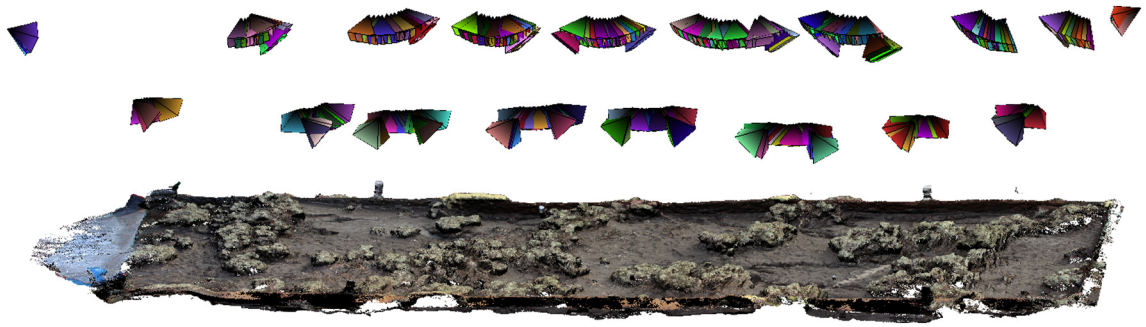

Fig. 3. Perspective view of a typical convergent image network used on an erosion plot showing camera locations and viewing directions represented by the colored pyramids above the reconstructed surface.

Ground control points (GCP) made of 16 mm white spheres mounted on a 0.15 m metal rod were aligned along the perimeter of each plot. A total of eight GCP were used on each plot and were surveyed using a Nikon NPR 352 total station (Nikon-Trimble Co. Ltd., Tokyo, Japan).

During the rainfall simulations, runoff discharge was monitored in a supercritical flume with a Teledyne 4230 flow meter (Isco, Inc., Linclon, Nebraska, USA). Flow depth measured by the Teledyne 4230 were converted into discharge (L/s) using a calibrated stage-discharge equation specific to the supercritical flume. Data from the flow meter was displayed in real-time on a computer screen for visual assessment of the hydrograph. The refresh rate of the flow meter was 0.06 Hz.

2.3. Rainfall simulation procedure and data

During each rainfall event, the time between the start of rainfall and the inception of runoff or time to runoff (*TTR*) was recorded. The duration of each run (*Rdur*) was a function of the time required to achieve steady state conditions. Rainfall was stopped when at least 10 min of trendless discharge was observed on the real-time hydrograph display.

Sediment samples were collected in 1 L bottles at a frequency of one sample every 3 min. Total sediment concentration was determined by decanting and drying runoff samples in an oven at 105 °C for 24 h. Manual discharge measurements were also made periodically (every 5–6 min) by recording the time needed to fill a 3.8 L bucket. This manual discharge measurement was used to verify and apply corrective measures when needed to the data collected by the flow meter.

The steady state runoff discharge Q_{ss}, was calculated from the hydrograph as the average discharge observed during the last 10 min of rainfall. Likewise, steady state sediment concentration *Sed* was calculated from sediment concentration measured during the same timeframe. Cumulative runoff *CumQ* and soil loss *CumS* were also calculated by integrating instantaneous runoff and sediment concentration through the runoff duration. Additional variables presented in this paper are *CumQ20* and *CumS20* which were respectively the cumulative runoff and sediment after 20 min of rainfall.

2.4. Microtopographic analysis

Before each rainfall simulation, a series of pictures were taken for the 3D reconstruction of plot pre-rainfall surface microtopography. These pre-rainfall reconstructions were differenced from the post-rainfall 3D models to assess the change in soil surface microtopography and estimate erosion and deposition. Post-rainfall images for the 3D reconstruction were taken 30 min after the rainfall was stopped. This delay was needed to promote infiltration and prevent the detrimental effect of ponding water on the 3D reconstruction quality.

The structure from motion software Agisoft PhotoScan 1.2 (Agisoft LLC, 2016) was used to reconstruct soil surface microtopography. Average, planimetric and vertical precisions estimated as the root mean square error of repeat measurements of GCP were respectively 1.4 mm and 0.6 mm. Orthophotos of each plot were produced and imported in ArcGIS (ESRI, 2011) to manually create polygons of the vegetation patches. These polygons were used as raster masks in the surface change analyses. The output of PhotoScan was a dense 3D point cloud which was interpolated into a 0.005 m grid spacing raster in ArcGIS to produce Digital Elevation Models (DEMs). DEMs corresponding to pre- and post-rainfall conditions were differenced and analyzed to describe sediment transport processes on each plot. Applying error propagation rules to the precision of the initial point clouds (0.6 mm), the difference maps produced from DEMs obtained at two epochs have a precision of 0.85 mm.

The methodology developed in Nouwakpo et al. (2017) to characterize various sediment transport processes with soil surface change metrics was also used in this paper. These metrics are volumes, average depths and ratios computed from the 3D data. Overall, plot-wide erosion and deposition processes were characterized to understand non-specific sediment transport dynamics as affected by vegetation treatments and other factors. In addition, the channel network was extracted from the original pre- and post-erosion DEMs and used to derive metrics characterizing sediment transport processes in concentrated flow pathways. Metrics quantifying erosion volumes and depths inform on detachment susceptibility controlled by a combined effect of erodibility, erosivity and availability. Metrics related to deposition volumes and depths in contrast characterize the transportability of detached material. Unlike the Nouwakpo et al. (2017) study, no DEM correction was made for clay expansion. The experiments were conducted at a period coinciding with the passage of a series of summer thunderstorms. Soils were therefore initially moist (8.7% volumetric moisture content on average), resulting in no appreciable soil swelling during the rainfall simulation experiments. The following areal and volumetric surface change metrics detailed in (Nouwakpo et al., 2017) were used in this study.

Volumes *TVE*, *TVD* and *TVN* correspond respectively to plot-wide erosion, deposition and net loss in m^3. As in Nouwakpo et al. (2017) flow concentration pathways were extracted by applying the bottom-hat operator to detect erosional features (Rodriguez et al., 2002; Schwanghart et al., 2013). The bottom-hat operator was used here as a feature extractor that detects and extracts local minima in the original DEMs using the following sequence of operations:

1- Create a 0.5 m by 0.5 m diamond-shaped structuring kernel
2- Apply a dilation operation on the original DEMs by moving the structuring element through the DEMs and in each window, replacing all cell values with the maximum value within the window
3- Apply a closing operation on the DEMs by eroding (similar to dilation but replacing all cell values with the minimum value within the window) the previously dilated DEMs
4- The bottom-hat maps were then generated as a subtraction between

the closed DEMs and the original DEMs. The average bottom-hat value in each map was used as a threshold to distinguish channel areas (< average bottom-hat value) from sheet and splash areas. Pre- and post-rainfall channels were then unified in one channel network for a plot.

Volumes of erosion (*CVE*), deposition (*CVD*) and net loss (*CVN*) within the channel network were then determined with pixels belonging to the channel network.

Volumes of erosion and deposition were normalized by the areas corresponding to these processes to obtain average depths of erosion *TZE* (m) and deposition *TZD* (m). In the channel network, these depths were labelled *CZE* (m) and *CZD* (m). Additional metrics were defined to characterize erosion, deposition and transport processes in each plot. The channel erosion ratio *CVR* expresses the proportion of total erosion that occurred within the channel network and was calculated as:

$$CVR = CVE/TVE \quad (1)$$

The total deposition ratio TDR describes the proportion of total erosion that is re-deposited within the plot and determined with the following equation:

$$TDR = TVD/TVE \quad (2)$$

The sediment delivery ratio SDR was defined as the ratio between the net erosion (erosion – deposition) and the total erosion.

$$SDR = TVN/TVE \quad (3)$$

2.5. Statistical analysis

Multiple linear regressions were used to evaluate the effect of vegetation cover on hydrology and erosion responses. Variables Q_{ss}, *Sed*, *CumQ*, *CumQ20*, *CumS* and *CumS20* were related to *Slope*, vegetation cover category (L, M or H), run duration *Rdur* and litter cover *Litter*. Surface change metrics were related to *Slope*, vegetation cover category, and cumulative runoff *CumQ*. In all multiple regressions, vegetation cover was used as a categorical variable with values L, M and H. The medium vegetation cover M was used as the reference to which L and H treatments were compared.

Before running a multiple linear regression, a Shapiro-Wilk test was performed on each explained variable to check for normality. Variables yielding a p-value < 0.1 were considered non-normal and were therefore normalized using a Box-Cox power transformation. The Variance Inflation Factor (VIF) was calculated for each factor and variable in the multiple linear regression and used to detect multi-collinearity between independent variables of the linear model. A VIF value greater or equal to 10 was used in this study to detect serious multi-collinearity. A stepwise regression was applied to each multiple regression to retain only explanatory variables influencing the coefficient of determination R^2. A pairwise student *t*-test was used to compare average slopes and litter cover across canopy cover groups. Statistical significance was defined in this paper at a level $\alpha = 0.05$.

3. Results

3.1. Effect of vegetation on soil loss and runoff generation

Boxplots of the distribution of litter cover and slope per canopy cover category are shown in Fig. 4. The p-values of the pairwise *t*-test of slope across canopy cover groups were respectively 0.16, 0.50 and 0.33 for the high-medium, high-low and medium-low comparisons. Slopes were therefore not statistically different between canopy cover groups as a result of the deliberate selection of plots on hillslopes of comparable steepness. While Fig. 4a shows an increasing tendency of litter with canopy cover, this trend was not statistically significant as p-values of the pairwise *t*-test were 0.78, 0.36 and 0.78 for the high-medium, high-low and medium-low comparisons. This lack of canopy cover effect on litter was likely due to the wide variability of litter cover in the high (H) canopy cover group and the overlapping range of litter in the low (L) and medium (M) groups (Fig. 4a). Tables 1 and 2 show respectively the results from the rainfall simulation experiment and the multiple linear regression analyses. Overall, rainfall simulations lasted 1891 ± 289 s (31.5 min) on average but differed in length based on vegetation cover density. Simulation duration *Rdur* differed based on cover density type with the longest simulations occurring on plots with H cover (2066 ± 408 s), the shortest simulations on L cover (1767 ± 195 s) and intermediate duration on plots with M cover (1841 ± 189 s). The statistical analysis in Table 2 shows however that litter and slope primarily controlled *Rdur* through positive relationships, an indication that litter and slope influenced the time needed for steady state runoff to develop. Furthermore, the time required for runoff initiation *TTR* was significantly delayed on the L plots (225 ± 25 s) compared to the M plots (132 ± 65 s) while the H plots had comparable TTR values (136 ± 33 s) to the M plots.

Fig. 5 shows runoff (Fig. 5a) and sediment (Fig. 5b) discharges averaged at regular time intervals from 0 to 1600 s across H, M and L plots. Hydrographs for M and L plots featured a unique increasing limb (Fig. 5a) while a bistage rising limb was observed for the H hydrograph (i.e. a rapid runoff initiation with sustained low runoff discharge until the 500 s mark followed by a rapid rise in discharge beyond 500 s). Fig. 5a also showed that steady state discharge was reached by the 1600 s mark for the M and L plots whereas runoff discharge for the H plots at the same mark was still gradually increasing. Sediment discharge graphs (Fig. 5b) mostly mimicked hydrographs but were characterized by a gradual decline in sediment discharge following a brief peak due to development of source-limiting conditions. The bistage hydrograph behavior noted for H plots was substantially muffled on the sediment discharge graph as the initial stage of runoff on H plots was associated with low erosion rates. A marked lag in sediment discharge increase was noted on the H plots compared to M and L plots and sediment discharge at runoff steady-state showed a distinctly greater sediment discharge on the high cover plots compared to both L and M plots.

Average steady-state discharge Q_{ss} for H, M and L vegetation covers were respectively 120 ± 18 mm/h, 110 ± 15 mm/h and 121 ± 15 mm/h while steady-state sediment concentrations *Sed* were 164.9 ± 48.4 g/L, 143.0 ± 18.4 g/L and 151.2 ± 13.0 g/L respectively for the same vegetation covers. The multiple linear regressions performed on Q_{ss} and *Sed* (Table 2) showed that no variable had a significant control on Q_{ss} while *Sed* was inversely controlled by litter cover and 36.1 g/L and greater on the H plots compared to the M plots.

The average cumulative runoff *CumQ* showed no statistically significant relationship with vegetation cover (Table 2). Average *CumQ* values were 46.5 ± 18 mm, 44.0 ± 10 mm and 41.3 ± 8 mm for H, M and L respectively. When the cumulative runoff after 20 min of rainfall *CumQ20* was considered, a significant (p-value = 0.010) decreasing effect ($R^2 = 0.56$) of canopy cover was observed (Fig. 6) which is consistent with the decreasing effect of H on *CumQ20* noted in Table 2. Cumulative sediment mass was on average greater on the H plots (93.3 ± 23.4 kg) than it was on M (79.4 ± 29.6 kg) and L (80.0 ± 22.5 kg) plots but these differences were not statistically significant and were not retained after the step-wise variable selection (Table 2). Similar to cumulative discharge, cumulative soil loss *CumS* was unrelated to canopy cover (Table 2). Unlike runoff however, this lack of vegetation effect was maintained on the cumulative soil loss at 20 min *CumS20* (Fig. 7). Both *CumQ* and *CumS* were primarily controlled by run duration *Rdur* due to the varying rainfall durations used in this study.

In our study, the rainfall depth at 5 min corresponds to the 25-year return depth for the area. Most plots at 5 min in the simulation were at the inception stage of runoff (Fig. 5). Average cumulative runoff measured at 5 min for H, M and L plots were respectively 0.4 ± 0.2 mm,

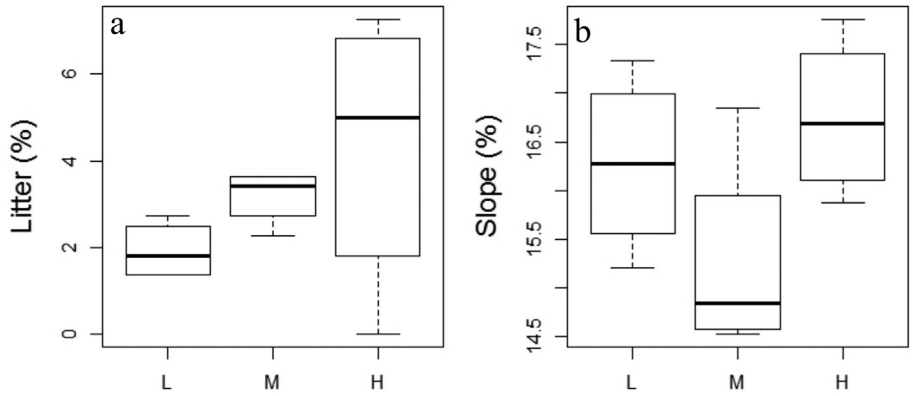

Fig. 4. Boxplot of litter cover (a) and slope (b) for canopy cover categories L (canopy cover < 5%), M (5% < canopy cover < 19%) and H (canopy cover > 19%).

Table 1
Results of the rainfall simulation experiment.

Plot	Cover category	*Slope* (%)	Canopy cover (%)	*Litter* (%)	*Rdur* (s)	*TTR* (s)	Ro. Dur (s)	*Qss* (mm/h)	*Sed* (g/L)	Total P (mm)	*CumQ* (mm)	Runoff ratio	*CumS* (kg)
1	H	17.0	19.1	7.3	2551.3	107.2	2515.8	134.6	122.3	80.8	66.6	0.82	122.9
2	H	16.3	21.4	6.4	2259.3	108.1	2186.2	131.4	127.3	71.5	56.6	0.79	96.7
3	H	15.8	22.3	3.6	1728.4	168.3	1617.5	120.4	188.0	54.7	36.7	0.67	87.0
4	H	17.7	26.9	0	1726.9	162.0	1562.0	94.9	222.2	54.7	26.3	0.48	66.5
5	M	14.5	5.9	3.2	1625.9	133.6	1490.9	116.2	156.3	51.5	39.9	0.78	76.6
6	M	16.8	5.0	3.6	2050.0	103.2	1993.1	108.8	155.5	64.9	54.1	0.83	115.0
7	M	14.6	12.3	3.6	1938.9	223.2	1757.2	126.0	143.3	61.4	49.5	0.81	83.4
8	M	15.0	13.2	2.3	1751.7	70.2	1728.1	90.5	116.8	55.5	32.5	0.59	42.7
9	L	17.3	1.8	2.7	1946.8	222.3	1767.2	104.8	165.7	61.6	43.2	0.70	94.7
10	L	16.6	1.8	1.4	1564.5	250.1	1354.0	130.7	151.4	49.5	35.9	0.72	71.0
11	L	15.2	3.2	2.3	1634.3	190.5	1515.0	109.9	134.3	51.8	34.6	0.67	52.7
12	L	15.9	2.7	1.4	1922.8	237.3	1733.7	138.9	153.6	60.9	51.5	0.85	101.9

Note: P is the total precipitation applied *TTR* is the time from the beginning of rainfall to the occurrence of runoff, *Rdur* is the duration of an entire experiment, Ro. Dur is the duration of runoff, Q_{ss} is the steady state discharge, *Sed* is the sediment concentration, *CumQ* is the total runoff volume and *CumS* is the cumulative soil loss.

1.3 ± 0.6 mm and 0.5 ± 0.3 mm and cumulative sediments were 0.1 ± 0.08 kg, 1.5 ± 1.3 kg and 0.3 ± 0.2 kg. The plots with high vegetation cover generated less runoff and less sediment than the medium and low cover plots. Nevertheless, the plots with medium cover had the highest runoff and sediment at the 5-minute mark due to an early rise of the hydrograph on these plots.

3.2. Effect of vegetation on 3D erosion and deposition volumes

Fig. 8a and b show respectively an example of hillshaded DEM before and after a rainfall event. From these maps one can note the effect of rainfall on the soil surface evidenced by a more pronounced channel network post-event (Fig. 8b). Fig. 8c and d show elevation difference as the result of the rainfall simulation on the example plot. Elevation differences in the entire plot are displayed in Fig. 8c while those within the channel network are shown in Fig. 8d. Average elevation losses corresponding to erosion processes ranged between 5.2 mm and 10.1 mm while deposition ranged between 2.1 mm and 7.7 mm. With a precision of change detection of 0.85 mm, the signal-to-noise ratio achieved in this study varied between 6 and 11.9 for erosion and between 2.5 and 9 for deposition, suggesting adequate ability to reliably discern elevation change patterns. The relationship between measured cumulative soil loss *CumS* and estimated 3D volume change is plotted in Fig. 9. Ideally, *CumS* should be equal to the product of *TVN* and soil bulk density. However, due to untraceable density changes between eroded and deposited material and the precision limit of the 3D reconstruction technique, the achieved R^2 between *CumS* and *TVN* was only 0.24. The R^2 doubled to 0.49 when deposition was excluded from the volume change estimation (*TVE*), perhaps because deposition is lower in magnitude compared to erosion and thus more deposition pixels occur within the precision limit of the 3D reconstruction. A soil bulk density of 1300 kg/m^3 translate the average net volume change into masses of 69.4 kg, 83.5 kg and 54.0 kg for L, M and H covers while these masses measured from runoff samples were 80.1 kg, 79.4 kg and 93.3 kg for the same cover categories.

Table 3 summarizes results of the multiple regression on surface change metrics. Vegetation cover had a significant effect on total erosion volumes *TVE* with high cover (H) having a statistically significant decreasing effect on *TVE* compared to the M cover. The cumulative runoff *CumQ* was also positively related to *TVE*. The average depth of erosion *TZE* was significantly lower for the low treatment (L) compared to the medium treatment (M) while no statistical difference was noted between H and M plots. Increase in *CumQ* were also associated with a significant increase in *TZE*. Even though cover had a decreasing effect on erosion volumes, *TZE* values show the opposite trend with L plots showing statistically lower *TZE* than M plots. However, there was no statistical distinction between M and H covers for *TZE*.

Deposition volumes *TVD* were primarily controlled by cover amount. The H cover had a significant promoting effect on deposition volumes compared to the M cover which had a similar effect as the L cover. When deposition volumes were normalized by deposition area, the resulting average deposition depth *TZD* was only a function of cover category. Deposition depths obtained for H plots were significantly higher than those of the M cover while the L plots were undiscernible from the M plots based. The proportion of eroded sediment that was redeposited, *TDR*, was dependent on cover amount and cumulative runoff *CumQ*. Cumulative runoff had a significant lowering effect on *TDR*. Vegetation cover amount had a positive influence on *TDR* with the H vegetation cover category showing significantly higher *TDR* values than the M cover category while the L cover class was statistically identical

Table 2
Multiple linear regression on time-to-runoff, run duration, discharge and sediment concentration using slope, litter, canopy cover and run duration as explanatory variables.

Explained variable	Explanatory variables	Coef.	Coef. p-value	VIF
TTR	Intercept	132.53	**2.3E-04**	
R^2 = 0.55	L	92.54	**0.02**	
	H	3.89	0.91	
Rdur	Intercept	−74.72	0.91	
R^2 = 0.80	*Slope*	99.49	**0.04**	1.00
	Litter	116.05	**4.0E-04**	1.00
Q_{ss}	Intercept	179.35	0.05	
R^2 = 0.48	Slope	−8.58	0.14	1.30
	L	21.88	0.10	1.17
	H	15.12	0.27	
	Rdur	0.03	0.09	1.17
Sed	Intercept	182.59	**1.7E-06**	
R^2 = 0.67	L	−7.30	0.63	1.07
	H	36.12	**0.04**	
	Litter	−12.45	**6.3E-03**	1.15
CumQ	Intercept	−20.77	0.16	
R^2 = 0.90	L	2.01	0.58	1.09
	H	−6.75	0.10	
	Rdur	0.03	**7.8E-03**	1.77
	Litter	1.86	0.18	1.81
CumQ20	Intercept	25.75	**4.6E-07**	
R^2 = 0.50	L	−1.83	0.54	
	H	−8.24	**0.02**	
CumS	Intercept	−36.85	0.27	
R^2 = 0.60	*Rdur*	0.064	**3.2E-03**	
CumS20	Intercept	−103.96	0.22	
R^2 = 0.38	Slope	10.10	0.08	1.25
	L	−11.68	0.34	1.12
	H	−24.02	0.10	1.12

Note: *TTR* is the time from the beginning of rainfall to the occurrence of runoff, *Rdur* is the duration of an experiment, Q_{ss} is the steady state discharge, *Sed* is the sediment concentration, *CumQ* is the total runoff volume and *CumS* is the cumulative soil loss. Vegetation treatments were L if canopy cover < 5%, M if 5% < canopy cover < 19% and H if canopy cover > 19%. Averages for L and H compared to the reference M.

to the M cover class. The high vegetation cover class also had a reducing effect on the sediment delivery ration *SDR*. *SDR* values were significantly lower on H plots than M plots. Net erosion *TVN* was a function of cover and cumulative runoff. Plots with high vegetation cover experienced more erosion than those with medium cover which were undistinguishable from plots with low cover.

Fig. 8b shows maps of channel networks delineated with the bottom-hat operator after each rainfall event. As illustrated in Fig. 8b, areas classified as concentrated flow also contain areas where visibly higher magnitudes of elevation change occurred. Average depth of erosion and deposition in these concentrated flow areas were respectively 8.2 mm and 5.2 mm vs. 6.7 mm and 4.5 mm plot-wide which is consistent with higher intensity fluvial processes in these plot regions compared to diffuse processes in the interrill areas included in the plot-wide metric. Since the bottom-hat operator makes no assumption of the magnitude of elevation change in the channel network delineation process, this result suggests that the bottom-hat operator was an adequate method to capture the channel network.

Results of the multiple regression on channel erosion and deposition metrics are presented in Table 4. Cumulative runoff mainly controlled erosion volumes *CVE* and depths *CZE* with no effect of vegetation cover class. Vegetation cover affected deposition volumes in the channel network. Both L and H cover plots experienced statistically higher deposition volumes than the M cover plots. When deposition volumes in the channel network were normalized by area, the ensuing deposition depth *CZD* showed a statistically significant increasing effect of the H vegetation cover class compared to the M cover class. The net erosion within the channel network *CVN* was mainly a function of cover and

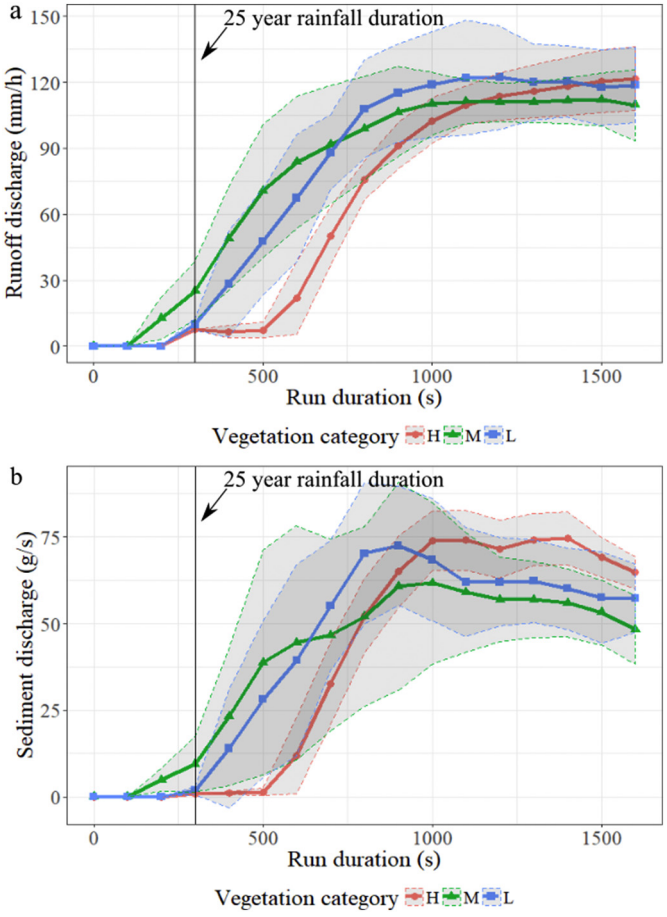

Fig. 5. Hydrographs (a) and sediment discharge graphs (b) obtained by averaging runoff and sediment discharges at regular time interval across treatments H (canopy cover > 19%), M (5% < canopy cover < 19%) and L (canopy cover < 5%). All simulations were truncated at 1600 s. The confidence band for each graph is marked by the grayed area.

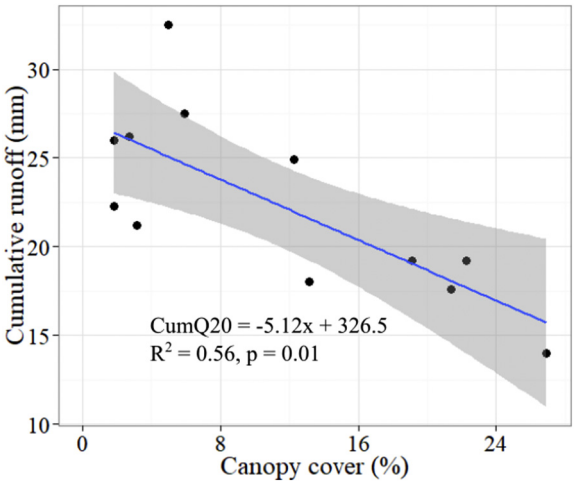

Fig. 6. Cumulative runoff after 20 min of rainfall simulation (CumQ20) as a function of canopy cover. The grayed area represents the confidence band.

cumulative runoff. *CVN* values were significantly lower for L and H covers than they were for M cover. Increase in cumulative runoff *CumQ* increased *CVN*. The ratio *CVR* of erosion volume in channels *CVE* over total erosion volume *TVE* was significantly affected by canopy cover with increase in canopy cover (H) associated with an increase in the proportion of channel erosion in total erosion.

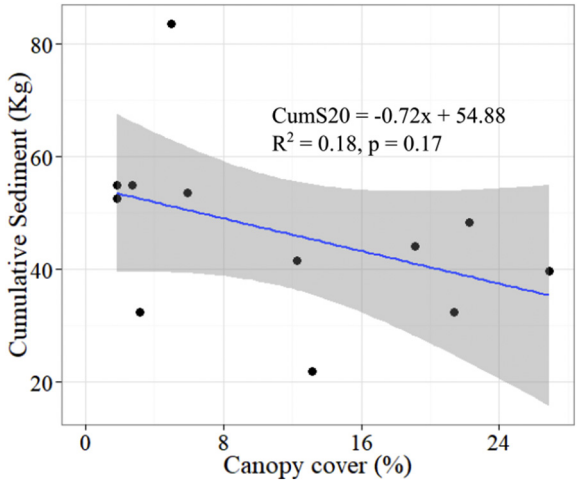

Fig. 7. Cumulative soil loss after 20 min of rainfall simulation (CumQ20) as a function of canopy cover. The grayed area represents the confidence band.

4. Discussions

4.1. Factors influencing runoff and erosion response

Measured steady state discharge (Q_{ss}) values in this study correspond to 120.3 mm/h, 110.4 mm/h and 121.1 mm/h of average runoff discharge, assuming even runoff generation over the 12 m^2 plot area for the high (H), medium (M) and low (L) cover categories. Observed runoff discharge values for H and L appeared higher than the applied rainfall intensity due to variations between target intensities set on the Walnut Gulch Rainfall Simulator (WGRS) and actual intensities delivered during the simulation. The WGRS is calibrated to deliver specific rainfall intensities at a nozzle pressure of 55 kPa set in the field with at pressure regulator. Nevertheless, on steep slopes (> 10%), downslope and upslope nozzles are at different hydraulic heads and a compensation was often needed to ensure that downslope nozzles approach the needed 55 kPa. This added compensation led to slight deviations of the actual intensity from the target intensity.

Another possible cause for instantaneous runoff rates higher than rainfall intensity, is the contribution of local storage and shallow subsurface flow to instantaneous runoff discharge. Local depressional storage on the plot especially at the beginning of runoff can gradually contribute to increased Q_{ss} values when the soil surface erodes, releasing previously stored water. In addition, the deepening rills during erosion lowers the water surface and thus the hydraulic potential along the rill. Water stored in the saturated adjacent subsurface zone can then re-emerge in the rills, contributing to increased instantaneous runoff discharge. In addition subsurface re-emergence at the downslope end of the plot is another potential contributor to the higher instantaneous runoff discharge compared to rainfall intensity. In our study, this contribution from depressional storage and subsurface re-emergence was not specifically measured but is expected to have only a marginal role in explaining the higher runoff rates than rainfall intensity measured for H and L.

In this study, we found that litter controlled the time required for runoff to reach steady-state conditions. Our results also indicate that steady-state runoff rate did not vary significantly between treatments. Litter promotes infiltration, reduces flow velocity (e.g., Li et al., 2011; Pierson et al., 2014) and limits raindrop-induced surface sealing (e.g., Pierson et al., 2013; Shin et al., 2013). In our study, greater soil surface exposure on the L plots likely resulted in the rapid development of surface sealing and associated rapid decrease in infiltration rate. On the M and H plots, higher litter and vegetation cover provided some protection against surface sealing, leading to a more gradual decline in infiltration rate. In addition, litter increases interception storage capacity (Williams et al., 2014b) which may have delayed the development of steady-state conditions.

Nevertheless, the positive effect of the vegetation and litter on infiltration processes conflicts with the significantly longer time to runoff *TTR* observed for the low vegetation plots (Table 2) compared to M and H plots. It is unclear what caused the shorter *TTR* observed on H and M plots but two hypotheses can be proposed. The first hypothesis attributes the significantly higher *TTR* values on L plots to differences in intrinsic soil properties on these plots. The soil on the L plots had a slightly lower clay content (15.4%) than soils on M (16.0%) and H (16.9%) but because clay contents were determined from a composite soil sample, the statistical significance of this difference is not known. While a lower clay content may facilitate infiltration processes, the magnitude of the difference in clay content between L and H plots seems unlikely to account for longer *TTR* on L plots. Furthermore, L plots had higher Sodium Adsorption Ratio (SAR) (SAR = 1.2) than M (SAR = 0.40) and H (SAR = 0.41) plots, again with no information on statistical significance of these differences. Increase in SAR is often associated with increased clay dispersion and decrease in infiltration rate (e.g., Bedbabis et al., 2014; Mamedov and Levy, 2001) which might account for the rapid increase of runoff discharge to steady-state on the L plots but not the longer *TTR* on these plots. Another hypothesis to explain the longer *TTR* on the L plots pertains to the dynamic of runoff flow in the interspace (space between vegetation patches). On average, the spatial extent of the interspace obtained by extracting vegetation patches from plot total area for H, M and L covers were respectively 69%, 88% and 96% of the plot area. Runoff and sediment transport preferentially occurs in the interspace and on the H and M plots leads to rapid flow concentration and greater flow depth compared to the L plots. As a result, runoff reached the plot end quicker on the H and M plots compared to L. The bistage hydrograph observed for the H plots supports this hypothesis since runoff within the narrow channels rapidly reached the plot end but did not carry enough erosive power to generate erosion. In the second stage of the H hydrograph increase, runoff from bare and vegetated sheet-and-splash areas started connecting with the channel network, leading to dramatic increases in runoff and enhanced erosion. It is important to note that neither hypothesis proposed here can be unequivocally verified with the data presented in this study but they are worth considering in the design of future investigations.

The 114 mm/h rainfall intensity applied in this study was estimated from the 25 year return period precipitation depth measured in 5 min (Bonnin et al., 2006). Because the rainfall duration in our experiments ranged from 26 to 42 min (or 49.5 mm to 80.8 mm), the actual return period of the precipitation applied was > 1000 years based on the Atlas 14 data (Bonnin et al., 2006). It is important to consider the spatial scale (12 m^2) at which measurements are being made in this study. At the 12 m^2 spatial scale, measurements made at an early stage of the hydrograph might not reliably inform runoff and erosion response during natural rainfall events. To relate our findings to natural processes, one must consider landscape position and topographic attributes of the plot being studied. Areas located at higher elevation of a drainage basin are less likely to receive upslope runon contributions compared to those located at lower elevations. Likewise, concave hillslopes will tend to concentrate more runoff and sediments and experience greater erosivity and sediment fluxes than convex landforms. It is therefore conceivable that during a 25-year storm, certain areas of the landscape would be receiving cumulative runoff and experiencing runoff erosive forces comparable to those applied in this study.

4.2. Vegetation and sediment transport processes

The higher 3D-estimated erosion depth (Table 3) on the medium and high cover plots compared to the low covers suggests that the potential reduction in rainsplash detachment due to increase in cover may have been partially compensated by incrementally greater and

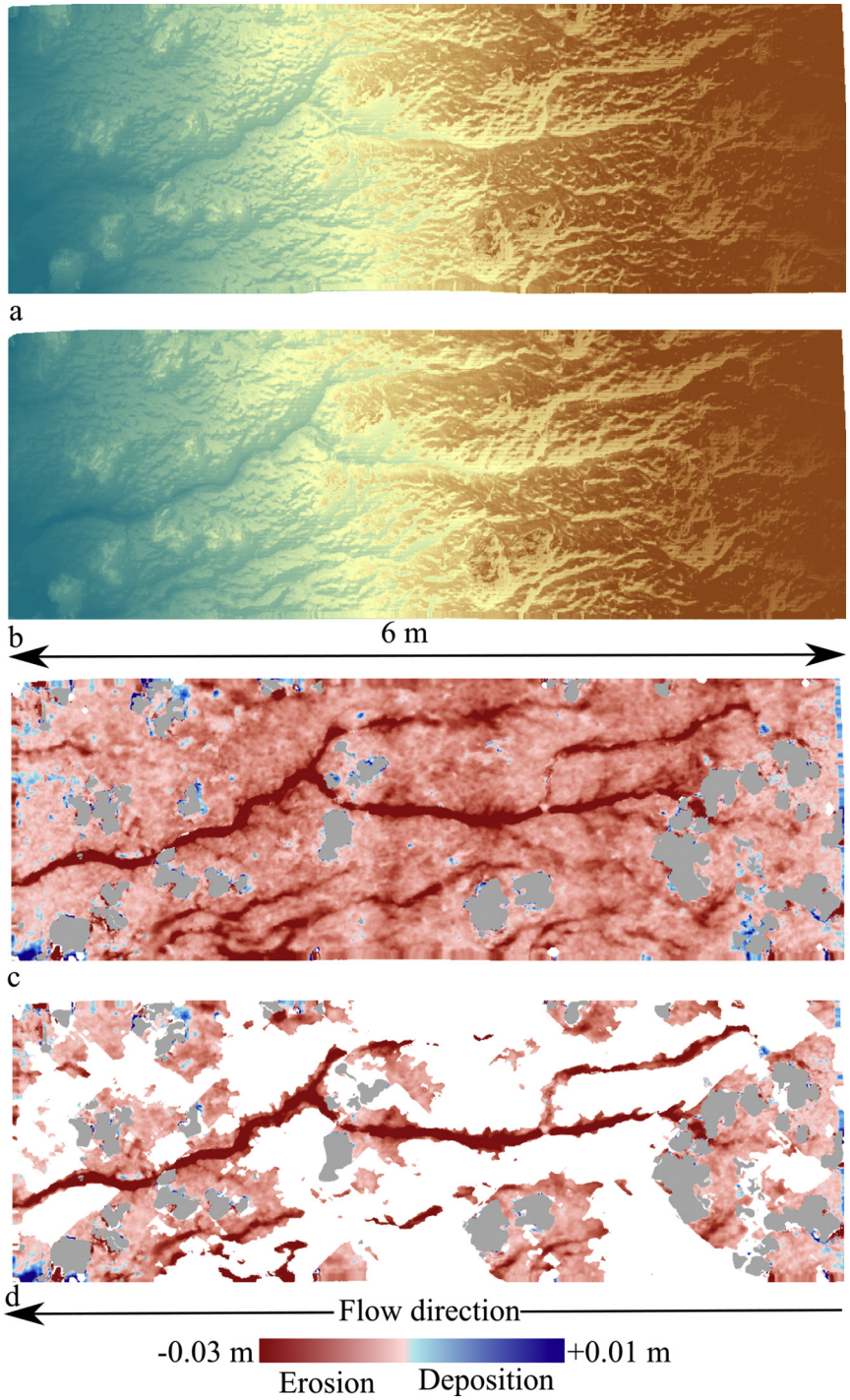

Fig. 8. Examples hillshaded maps before rainfall (a), after rainfall (b) and elevation differences across the entire plot (c) and in the delineated channel network (d). Gray polygons in the difference maps mark the outlines of plant canopies. For this example plot, slope = 16.8%, plant canopy cover = 5.0%.

more erosive flow depths as runoff was channeled in the narrower interspaces of the high cover plots. This may have led to the higher sediment concentration on the high cover plots and to the lack of statistical effect of vegetation on cumulative soil loss at the 20 min mark. In other studies using 3D data to understand erosion processes on sparsely vegetated shrubland, average erosion depth was found to be inversely related to vegetation cover (e.g., Nouwakpo et al., 2016b; Nouwakpo et al., 2017). Nevertheless, the lower total erosion volume TVE on the high cover plots suggests that soil cover protection by vegetation reduced the areas available for active erosion. An increase in erosion depth with vegetation contrasts with the traditionally perceived reduction effect of vegetation on erosion processes (e.g., Al-Hamdan et al., 2012; Zhang et al., 2017) and highlights the need for more research combining 3D reconstruction technologies with runoff measurements.

As illustrated in Fig. 9, soil loss measurement from runoff samples as a reference measure of erosion is still difficult to match by common 3D reconstruction techniques due to factors including soil density changes and precision limit of the 3D reconstruction technique. Hänsel et al. (2016) noted that increase in density due to raindrop-induced compaction on tilled plots partially accounted for observed discrepancies between 3D-estimated and runoff sediment samples. In our study, such

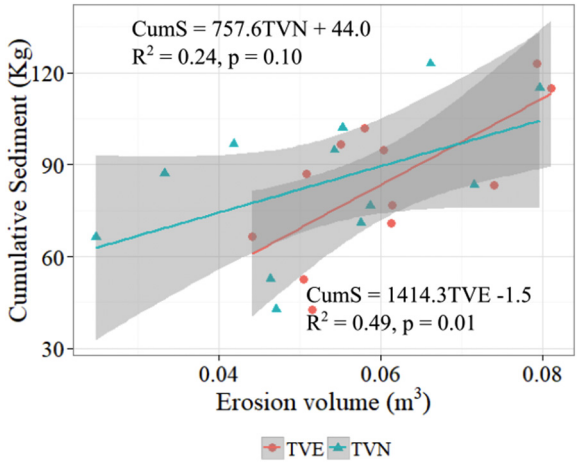

Fig. 9. Cumulative soil loss as a function of 3D volume change. *TVE* is the volume (m^3) of erosion and *TVN* the net volume change (Erosion-Deposition) in m^3. The grayed area represents the confidence band.

Table 3
Multiple linear regression on plot-wide erosion and deposition volumes and depths.

Explained variable	Explanatory variables	Coef.	Coef. p-value	VIF
TVE	Intercept	−0.02	0.58	–
R^2 = 0.82	Slope	3.5E-03	0.16	1.26
	L	−0.01	0.06	1.13
	H	−0.02	**0.02**	1.13
	CumQ	6.4E-05	**2.2E-03**	1.02
*TZE**	Intercept	−42,989.13	**8.4E-03**	–
R^2 = 0.89	Slope	1148.30	0.18	1.26
	L	−5507.68	**0.02**	1.13
	H	1725.75	0.40	1.13
	CumQ	20.12	**3.9E-03**	1.02
*TVD**	Intercept	−8.90	**2.8E-05**	–
R^2 = 0.90	L	1.20	0.08	1.01
	H	4.81	**4.1E-05**	1.01
	CumQ	−3.9E-03	0.06	1.02
*TZD**	Intercept	−12.54	**9.3E-11**	
R^2 = 0.86	L	−1.22	0.05	
	H	2.61	**8.0E-04**	
TVN	Intercept	−0.02	0.56	–
R^2 = 0.89	Slope	3.0E-03	0.23	1.26
	L	−0.01	0.06	1.13
	H	−0.03	**1.2E-03**	1.13
	CumQ	7.6E-05	**9.2E-04**	1.02
*TDR**	Intercept	−2.12	**3.1E-03**	–
R^2 = 0.91	L	0.65	0.05	1.01
	H	2.46	**2.8E-05**	1.01
	CumQ	−3.0E-03	**9.0E-03**	1.02
*SDR**	Intercept	−0.10	**1.5E-04**	–
R^2 = 0.96	L	−0.02	0.08	1.01
	H	−0.11	**1.4E-06**	1.01
	CumQ	1.2E-04	**2.1E-03**	1.02

Note: *TVE*, *TVD* are volumes (m^3) of erosion and deposition and *TVN* is the net volume (m^3) change (Erosion-Deposition); *TZE* and *TZD* are average depths (m) of erosion and deposition; *TDR* is the ratio of deposition over erosion volumes (*TVD/TVE*) and SDR is the sediment delivery ratio (*TVN/TVE*). Variables marked with an asterisk (*) have been normalized through a Box-Cox power transformation. Vegetation treatments were L if canopy cover < 5%, M if 5% < canopy cover < 19% and H if canopy cover > 19%. Averages for L and H compared to the reference M.

raindrop-induced increase in density was not expected because the soil surface was consolidated by a contemporaneous series of natural rainfall events. In addition, prior studies in the same environment (Nouwakpo et al., 2017) have described a decrease in density due to clay expansion when rainfall simulations were conducted on dry soils.

Table 4
Multiple linear regression on erosion and deposition volumes and depths within channels.

Explained variable	Explanatory variables	Coef.	Coef. p-value	VIF
CVE	Intercept	−0.01	0.62	–
R^2 = 0.74	Slope	2.1E-03	0.20	1.26
	L	−7.1E-03	0.06	1.13
	H	−2.3E-03	0.55	1.13
	CumQ	2.8E-05	**0.02**	1.02
CZE	Intercept	3.2E-03	0.05	–
R^2 = 0.71	L	−2.5E-04	0.76	1.01
	H	1.2E-03	0.16	1.01
	CumQ	8.8E-06	**7.5E-03**	1.02
CVD*	Intercept	−7.85	**2.1E-06**	–
R^2 = 0.98	L	1.12	**0.02**	1.01
	H	3.55	**1.2E-05**	1.01
	CumQ	−2.5E-03	0.06	1.02
CZD*	Intercept	−11.98	**9.2E-11**	–
R^2 = 0.92	L	−1.02	0.07	–
	H	2.45	**9.0E-04**	–
CVN*	Intercept	−0.01	0.48	–
R^2 = 0.85	Slope	1.8E-03	0.17	1.26
	L	−8.1E-03	**0.02**	1.13
	H	−0.01	**5.5E-03**	1.13
	CumQ	3.6E-05	**2.0E-03**	1.02
CVR	Intercept	0.60	**5.6E-06**	–
R^2 = 0.77	L	−0.03	0.44	1.01
	H	0.13	**3.8E-03**	1.01
	CumQ	−1.6E-04	0.14	1.02

Note: *CVE*, *CVD* are volumes (m^3) of erosion and deposition and *CVN* is the net volume (m^3) change (Erosion-Deposition); *CZE* and *CZD* are average depths (m) of erosion and deposition; *CVR* is the volume-based ratio of channel erosion *CVE* over total plot erosion *TVE* (*CVE/TVE*). Variables marked with an asterisk (*) have been normalized through a Box-Cox power transformation. Vegetation treatments were L if canopy cover < 5%, M if 5% < canopy cover < 19% and H if canopy cover > 19%. Averages for L and H compared to the reference M.

In the current study however, initial soil moisture was higher compared to the (Nouwakpo et al., 2017) due to the natural rainfall events that preceded the experiments. Another potential cause of discrepancy between 3D data and runoff-measured soil loss in our study is that vegetation patches were excluded from the 3D analysis due to high reconstruction noise in these patches. Nevertheless, surface change metrics (volumes, depths and ratios) derived from the 3D data captured in detail the effect of vegetation on detachment and transport processes while the lumped soil loss measured from the runoff samples did not inform on the nature and extent of surface processes at play in each plot. This result highlights the advantage of combining traditional soil loss data with surface change metrics acquired with microtopographic survey. Both soil loss measurement by runoff sampling and 3D reconstructions are thus complementary for a detail understanding of erosion and sediment transport processes.

Vegetation explained only 25% of the variability in the average erosion depth *TZE* and 86% of the variability in average deposition depth *TZD*. As a result, net soil erosion was reduced by vegetation primarily due to its promoting effect on deposition. This finding is consistent with results from a previous study (Nouwakpo et al., 2017) conducted at two sites in the same saline environment and has important implications in managing these ecosystems. The effects of vegetation on *TVD*, *TZD*, *TVN*, *TDR* and *SDR* suggest that vegetation reduced transport efficiency of sediments on the hillslope by promoting deposition of detached sediments. As noted in.

Fig. 8, deposition tends to occur at the periphery of shrubs and this is consistent with the depositional features associated with the deflection of fluvial runoff by vegetation patches described by others (e.g., Meire et al., 2014; Rominger and Nepf, 2011).

Along with sediments, one can imagine greater runoff infiltration at the periphery of vegetation features. Our study demonstrated that

vegetation impacted the cumulative runoff after 20 min of simulation by delaying the onset of sustained runoff generation from vegetated patches. This finding is consistent with those from other studies in similar sparsely vegetated environments where vegetation was found to decrease runoff (e.g., Bergkamp, 1998; Cerda, 1997; Puigdefabregas et al., 1999). While not specifically measured in this study, it is likely that favorable soil properties in vegetation patches resulted in greater infiltration and storage similar to that described by Cerda (1997). Nevertheless, our study revealed that vegetation did not influence steady state runoff discharge rate, suggesting that total vegetation cover alone was not sufficient to significantly reduce instantaneous runoff rate. In effect, our site was shrub-dominated with nearly 100% of the canopy cover composed of a few shrub species, resulting in well-connected interspaces. As shown in the concentrated flow 3D data in this paper, the higher vegetation cover H was associated with a higher ratio of concentrated flow *CVR*, suggestive of runoff being concentrated in the narrower interspace. Various authors have noted the importance of spatial and process (sheet and splash, concentrated flow erosion, etc.) connectivity in the hydrologic and erosion response of arid and semi-arid rangelands (e.g., Tongway and Ludwig, 1997; Wainwright et al., 2000; Williams et al., 2016a). In the shrub-dominated landscape where this study was conducted, little herbaceous existed between the shrubs, leading to continuously connected bare interspaces where runoff could rapidly concentrate and exit the hillslope. Our study demonstrates the importance of total vegetation cover in controlling runoff and erosion but also highlights the crucial role that diversity in vegetation life form might play in resource fluxes in these sparsely vegetated systems. Further research might need to elucidate the effect of vegetation composition and spatial arrangement on transport processes.

5. Conclusions

In this study, we found vegetation to be linked to soil erosion, runoff generation and sediment transport processes through a series of complex interactions between physical processes and biotic attributes. Rainfall duration which was primarily controlled by both the time required before the inception of runoff and that needed to achieve steady-state was a positive function of litter cover and slope. Cumulative runoff after 20 min of rainfall showed that increase in vegetation cover delayed the rapid increase in runoff, during the rising stage of the hydrograph, leading to lower cumulative runoff. Cumulative sediment at 20 min of rainfall did not show a significant effect of vegetation. Vegetation did not significantly affect steady-state discharge but plant litter significantly reduced rainsplash and lowered sediment concentration. Data from the 3D reconstruction analysis showed that vegetation mainly controlled net sediment transport in and out the channel network by primarily acting on deposition processes. Vegetation cover lowered 3D-estimated total erosion volumes but increased average erosion depth, consistent with an increase in runoff flow depth and thus erosivity as runoff was concentrated in the reduced interspace between vegetation patches. This finding in the 3D data was further supported by higher sediment concentration observed on plots with high vegetation cover. This study highlights the need for more research combining 3D reconstructions with traditional soil erosion assessment methods to further clarify links between of sediment transport processes and land surface conditions.

Acknowledgements

This study was funded by the US DOI Bureau of Reclamation, Bureau of Land Management, USDA Agricultural Research Service (Cooperative Agreement 59-2060-5-002). USDA is an equal opportunity provider and employer. Mention of a proprietary product does not constitute a guarantee or warranty of the product by USDA or the authors, and it does not imply its approval to the exclusion of the other products that also may be suitable.

References

Abrahams, A.D., Parsons, A.J., Wainwright, J., 1995. Effects of vegetation change on interrill runoff and erosion, walnut gulch, southern Arizona. Geomorphology 13, 37–48.
Agisoft LLC, 2016. Agisoft PhotoScan Professional Edition. Agisoft LLC, Russia (pp. Commercial SFM software).
Al-Hamdan, O.Z., et al., 2012. Characteristics of concentrated flow hydraulics for rangeland ecosystems: implications for hydrologic modeling. Earth Surf. Process. Landf. 37, 157–168.
Al-Hamdan, O.Z., et al., 2013. Risk assessment of erosion from concentrated flow on rangelands using overland flow distribution and shear stress partitioning. Trans. ASABE 56, 539–548.
Bedbabis, S., Ben Rouina, B., Boukhris, M., Ferrara, G., 2014. Effect of irrigation with treated wastewater on soil chemical properties and infiltration rate. J. Environ. Manag. 133, 45–50.
Bergkamp, G., 1998. A hierarchical view of the interactions of runoff and infiltration with vegetation and microtopography in semiarid shrublands. Catena 33, 201–220.
Bhark, E.W., Small, E.E., 2003. Association between plant canopies and the spatial patterns of infiltration in shrubland and grassland of the Chihuahuan Desert, New Mexico. Ecosystems 6, 185–196.
Blackburn, W.H., 1975. Factors influencing infiltration rate and sediment production of semiarid rangelands in Nevada. Water Resour. Res. 11, 929–937.
Bonnin, G.M., et al., 2006. Precipitation-frequency atlas of the United States. In: NOAA atlas, pp. 14.
Bracken, L.J., Croke, J., 2007. The concept of hydrological connectivity and its contribution to understanding runoff-dominated geomorphic systems. Hydrol. Process. 21, 1749–1763.
Buis, E., Veldkamp, A., 2008. Modelling dynamic water redistribution patterns in arid catchments in the Negev Desert of Israel. Earth Surf. Process. Landf. 33, 107–122.
Cadaret, E.M., Mcgwire, K.C., Nouwakpo, S.K., Weltz, M.A., Saito, L., 2016. Vegetation canopy cover effects on sediment erosion processes in the Upper Colorado River Basin Mancos shale formation, price, Utah, USA. Catena 147, 334–344.
Caldwell, T.G., Young, M.H., McDonald, E.V., Zhu, J.T., 2012. Soil heterogeneity in Mojave Desert shrublands: biotic and abiotic processes. Water Resour. Res. 48, 12.
Cammeraat, L.H., Imeson, A.C., 1998. Deriving indicators of soil degradation from soil aggregation studies in southeastern Spain and southern France. Geomorphology 23, 307–321.
Carlyle-Moses, D.E., 2004. Throughfall, stemflow, and canopy interception loss fluxes in a semi-arid Sierra Madre Oriental matorral community. J. Arid Environ. 58, 181–202.
Cerda, A., 1997. The effect of patchy distribution of Stipa tenacissima L on runoff and erosion. J. Arid Environ. 36, 37–51.
Cerdan, O., Le Bissonnais, Y., Souchere, V., Martin, P., Lecomte, V., 2002. Sediment concentration in interrill flow: interactions between soil surface conditions, vegetation and rainfall. Earth Surf. Process. Landf. 27, 193–205.
Chartier, M.P., Rostagno, C.M., 2006. Soil erosion thresholds and alternative states in northeastern Patagonian rangelands. Rangel. Ecol. Manag. 59, 616–624.
Emmett, W.W., 1970. The Hydraulics of Overland Flow on Hillslopes. US Govt. Print. Off, pp. 2330–7102.
ESRI, 2011. ArcGIS Desktop Release 10. Evironmental Systems Research Institute, Redlands, CA.
Gholami, L., Sadeghi, S.H., Homaee, M., 2013. Straw mulching effect on splash erosion, runoff, and sediment yield from eroded plots. Soil Sci. Soc. Am. J. 77, 268–278.
Gillan, J.K., Karl, J.W., Barger, N.N., Elaksher, A., Duniway, M.C., 2016. Spatially explicit rangeland erosion monitoring using high-resolution digital aerial imagery. Rangel. Ecol. Manag. 69, 95–107.
Hänsel, P., Schindewolf, M., Eltner, A., Kaiser, A., Schmidt, J., 2016. Feasibility of high-resolution soil erosion measurements by means of rainfall simulations and SfM photogrammetry. Hydrology 3, 38.
Herrick, J.E., Bestelmeyer, B.T., Archer, S., Tugel, A.J., Brown, J.R., 2006. An integrated framework for science-based arid land management. J. Arid Environ. 65, 319–335.
Li, X.Y., et al., 2011. Controls of infiltration-runoff processes in Mediterranean karst rangelands in SE Spain. Catena 86, 98–109.
Magliano, P.N., Breshears, D.D., Fernandez, R.J., Jobbagy, E.G., 2015. Rainfall intensity switches ecohydrological runoff/runon redistribution patterns in dryland vegetation patches. Ecol. Appl. 25, 2094–2100.
Mamedov, A.I., Levy, G.J., 2001. Clay dispersivity and aggregate stability effects on seal formation and erosion in effluent-irrigated soils. Soil Sci. 166, 631–639.
Meire, D., Kondziolka, J.M., Nepf, H.M., 2014. Interaction between neighboring vegetation patches: impact on flow and deposition. Water Resour. Res. 50, 3809–3825.
Merino-Martín, L., et al., 2012. Ecohydrological source-sink interrelationships between vegetation patches and soil hydrological properties along a disturbance gradient reveal a restoration threshold. Restor. Ecol. 20, 360–368.
Nearing, M.A., et al., 2011. A rangeland hydrology and erosion model. Trans. ASABE 54, 901–908.
Nicolau, J.M., Solebenet, A., Puigdefabregas, J., Gutierrez, L., 1996. Effects of soil and vegetation on runoff along a catena in semi-arid Spain. Geomorphology 14, 297–309.
Nouwakpo, S.K., Weltz, M.A., McGwire, K., 2016a. Assessing the performance of structure-from-motion photogrammetry and terrestrial LiDAR for reconstructing soil surface microtopography of naturally vegetated plots. Earth Surf. Process. Landf. 41, 308–322.
Nouwakpo, S.K., Weltz, M., Hernandez, M., Champa, T., Fisher, J., 2016b. Performance of the rangeland hydrology and erosion model for runoff and erosion assessment on a semiarid reclaimed construction site. J. Soil Water Conserv. 71, 220–236.
Nouwakpo, S.K., Weltz, M.A., McGwire, K.C., Williams, J.C., Osama, A.-H., Green,

C.H.M., 2017. Insight into sediment transport processes on saline rangeland hillslopes using three-dimensional soil microtopography changes. Earth Surf. Process. Landf. 42, 681–696.
Nulsen, R.A., Bligh, K.J., Baxter, I.N., Solin, E.J., Imrie, D.H., 1986. The fate of rainfall in a mallee and heath vegetated catchment in southern Western Australia. Aust. J. Ecol. 11, 361–371.
Owens, M.K., Lyons, R.K., Alejandro, C.L., 2006. Rainfall partitioning within semiarid juniper communities: effects of event size and canopy cover. Hydrol. Process. 20, 3179–3189.
Paige, G.B., Stone, J.J., Smith, J.R., Kennedy, J.R., 2004. The walnut gulch rainfall simulator: a computer-controlled variable intensity rainfall simulator. Appl. Eng. Agric. 20, 25–31.
Parsons, A.J., Abrahams, A.D., Simanton, J.R., 1992. Microtopography and soil-surface materials on semi-arid piedmont hillslopes, southern Arizona. J. Arid Environ. 22, 107–115.
Pierson, F.B., Bates, J.D., Svejcar, T.J., Hardegree, S.P., 2007. Runoff and erosion after cutting western juniper. Rangel. Ecol. Manag. 60, 285–292.
Pierson, F.B., Moffet, C.A., Williams, C.J., Hardegree, S.P., Clark, P.E., 2009. Prescribed-fire effects on rill and interrill runoff and erosion in a mountainous sagebrush landscape. Earth Surf. Process. Landf. 34, 193–203.
Pierson, F.B., et al., 2010. Hydrologic vulnerability of sagebrush steppe following pinyon and juniper encroachment. Rangel. Ecol. Manag. 63, 614–629.
Pierson, F.B., et al., 2013. Hydrologic and erosion responses of sagebrush steppe following juniper encroachment, wildfire, and tree cutting. Rangel. Ecol. Manag. 66, 274–289.
Pierson, F.B., Williams, C.J., Kormos, P.R., Al-Hamdan, O.Z., 2014. Short-term effects of tree removal on infiltration, runoff, and erosion in woodland-encroached sagebrush steppe. Rangel. Ecol. Manag. 67, 522–538.
Polyakov, V.O., Nearing, M.A., Stone, J.J., Collins, C.D.H., Nichols, M.H., 2016. Quantifying decadal-scale erosion rates and their short-term variability on ecological sites in a semi-arid environment. Catena 137, 501–507.
Prosdocimi, M., et al., 2017. Rainfall simulation and structure-from-motion photogrammetry for the analysis of soil water erosion in Mediterranean vineyards. Sci. Total Environ. 574, 204–215.
Puigdefabregas, J., Sole, A., Gutierrez, L., del Barrio, G., Boer, M., 1999. Scales and processes of water and sediment redistribution in drylands: results from the Rambla Honda field site in Southeast Spain. Earth Sci. Rev. 48, 39–70.
Rodriguez, F., Maire, E., Courjault-Radé, P., Darrozes, J., 2002. The black top hat function applied to a DEM: a tool to estimate recent incision in a mountainous watershed (Estibère watershed, central Pyrenees). Geophys. Res. Lett. 29, 9–1-9-4.
Rogers, R.D., Schumm, S.A., 1991. The effect of sparse vegetative cover on erosion and sediment yield. J. Hydrol. 123, 19–24.
Rominger, J.T., Nepf, H.M., 2011. Flow adjustment and interior flow associated with a rectangular porous obstruction. J. Fluid Mech. 680, 636–659.
Rostagno, C.M., Delvalle, H.F., 1988. Mounds associated with shrubs in aridic soils of the Northeastern Patagonia: characteristics and probable genesis. Catena 15, 347–359.
Sadeghi, S.H.R., Seghaleh, M.B., Rangavar, A.S., 2013. Plot sizes dependency of runoff and sediment yield estimates from a small watershed. Catena 102, 55–61.
Schlesinger, W.H., et al., 1990. Biological feedbacks in global desertification. Science (Washington) 247, 1043–1048.
Schwanghart, W., Groom, G., Kuhn, N.J., Heckrath, G., 2013. Flow network derivation from a high resolution DEM in a low relief, agrarian landscape. Earth Surf. Process. Landf. 38, 1576–1586.
Shin, S.S., Park, S.D., Lee, K.S., 2013. Sediment and hydrological response to vegetation recovery following wildfire on hillslopes and the hollow of a small watershed. J. Hydrol. 499, 154–166.
Siepel, A.C., Steenhuis, T.S., Rose, C.W., Parlange, J.Y., McIsaac, G.F., 2002. A simplified hillslope erosion model with vegetation elements for practical applications. J. Hydrol. 258, 111–121.
Tongway, D.J., Ludwig, B., 1997. The nature of landscape dysfunction in rangelands. In: Ludwig, B., Tongway, D.J., Freudenberger, D., Noble, J., Hodgkinson, K.C. (Eds.), Landscape Ecology, Function and Management: Principles from Australia's Rangelands. CISRO, Melbourne, Australia, pp. 49–61.
Turnbull, L., et al., 2012. Understanding the role of ecohydrological feedbacks in ecosystem state change in drylands. Ecohydrology 5, 174–183.
VanAmburg, L., Booth, D., Weltz, M., Trlica, M., 2005. A laser point frame to measure cover. Rangel. Ecol. Manag. 58, 557–560.
Wainwright, J., Parsons, A.J., Abrahams, A.D., 2000. Plot-scale studies of vegetation, overland flow and erosion interactions: case studies from Arizona and New Mexico. Hydrol. Process. 14, 2921–2943.
Wang, B., et al., 2014. Effects of near soil surface characteristics on soil detachment by overland flow in a natural succession grassland. Soil Sci. Soc. Am. J. 78, 589–597.
Whitford, W.G., Martinez-Turanzas, G., Martinez-Meza, E., 1995. Persistence of desertified ecosystems: explanations and implications. Environ. Monit. Assess. 37, 319–332.
Williams, C.J., et al., 2014a. Can wildfire serve as an ecohydrologic threshold- reversal mechanism on juniper- encroached shrublands. Ecohydrology 7, 453–477.
Williams, C.J., Pierson, F.B., Robichaud, P.R., Boll, J., 2014b. Hydrologic and erosion responses to wildfire along the rangeland-xeric forest continuum in the western US: a review and model of hydrologic vulnerability. Int. J. Wildland Fire 23, 155–172.
Williams, C.J., et al., 2016a. Structural and functional connectivity as a driver of hillslope erosion following disturbance. Int. J. Wildland Fire 25, 306–321.
Williams, C.J., et al., 2016b. Incorporating hydrologic data and ecohydrologic relationships into ecological site descriptions. Rangel. Ecol. Manag. 69, 4–19.
Zhang, K.D., Wang, Z.G., Wang, G.Q., Sun, X.M., Cui, N.B., 2017. Overland-flow resistance characteristics of nonsubmerged vegetation. J. Irrig. Drain. Eng. 143.